Measurement Of Quasiparticle Transport In Aluminum Films Using Tungsten Transition-Edge Sensors

J.J. Yen,[1, a)] B. Shank,[1] B.A. Young,[2] B. Cabrera,[1] P.L. Brink,[3] M. Cherry,[3] J.M. Kreikebaum,[1, 2] R. Moffatt,[1] P. Redl,[1] A. Tomada,[3] and E.C. Tortorici[2]

[1)] *Department of Physics, Stanford University, Stanford, CA 94305, USA*

[2)] *Department of Physics, Santa Clara University, CA 95053, USA*

[3)] *SLAC National Accelerator Laboratory, 2575 Sand Hill Road, Menlo Park, CA 94025, USA*

(Dated: 10 October 2014)

We report on experimental studies of phonon sensors which utilize quasiparticle diffusion in thin aluminum films connected to tungsten transition-edge-sensors (TESs) operated at 35 mK. We show that basic TES physics and a simple physical model of the overlap region between the W and Al films in our devices enables us to accurately reproduce the experimentally observed pulse shapes from x-rays absorbed in the Al films. We further estimate quasiparticle loss in Al films using a simple diffusion equation approach. These studies allow the design of phonon sensors with improved performance.

Quasiparticle transport dynamics have been studied experimentally by many groups[1–3] using different materials, fabrication processes, and readout schemes. Quasiparticle transport in Al films plays an important role in the design specifications of Cryogenic Dark Matter Search (CDMS) detectors[4]. These detectors utilize photolithographically patterned films of sputtered Al and W on both sides of high-purity, kg-scale, Ge and Si crystals. The superconducting Al and W films perform two roles simultaneously: some absorb phonon energy and others serve as ionization collection electrodes.

When a particle interacts with a CDMS detector, electron-hole pairs and phonons are created. Under typical operating conditions, a ∼1V/cm bias is used to drift the e-/h+ pairs through the bulk of the crystal so charge can be collected at the detector surfaces. At the same time, the athermal phonons produced by the event make their way to the detector surfaces where they can be absorbed in the Al film by breaking Cooper pairs which create quasiparticles. Ideally, the quasiparticles diffuse randomly in the Al until they get trapped in the overlap region between the Al and W films, where the superconducting energy gap is smaller than in the Al film alone[5]. This trapped energy gets absorbed by an attached W-TES, adding heat and providing the detector's phonon signal for that event. We call these phonon sensors Quasiparticle-trap-assisted-Electrothermal-feedback Transition-edge-sensors (QETs)[6].

The quasiparticle (qp) trapping length in CDMS Al films impacts overall detector energy performance. Here we present results from a detailed study of energy collection and qp propagation in Al films coupled to W-TESs and describe an innovative model that explains QET pulse shapes and overall performance, and provides a way to measure qp trapping lengths in thin films and the energy transport efficiency from the qp energy to the TES electron system. Our measurements have benefited from a signal analysis approach based on template matching rather than pulse integration which improves our energy resolution by a factor of two and yields better event reconstruction overall[7].

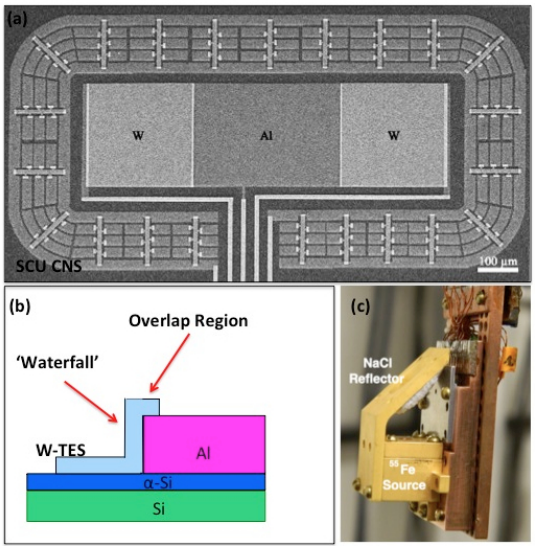

FIG. 1: (Color online) (a) SEM image of Al/W test device. The W-TESs at the ends of the Al film are 250μm x 250μm. The racetrack-shaped outer channel acts as a veto for substrate events. (b) Schematic side view (not to scale) where each W-TES overlaps the Al film. (c) Sample mount with ^{55}Fe / NaCl x-ray fluorescence source. The test device is hidden behind a collimator plate.

Test samples consisted of photolithographically patterned, 300 nm-thick Al and 40 nm-thick W films. Three Al film lengths were studied: 250μm, 350μm and 500μm. The metallization and process steps were identical to those used for CDMS detectors, including a 40 nm layer of amorphous Si (aSi) sputtered on each cleaned Si substrate just prior to metallization. Fig. 1a shows an image

[a)] Email address: jeffyen@stanford.edu

of one test device with a central 250 μm-wide x 350 μm-long Al phonon absorption film coupled to 250 μm x 250 μm W TESs (W-TES1 and W-TES2) at either end. A distributed racetrack-like outer TES channel (W-TES3) served as a veto against substrate events. A schematic diagram of the film geometry at the overlap regions between the W-TESs and the Al energy collection film is shown in Fig. 1b. Fig. 1c shows the OFHC Cu structure used to both anchor devices to the mixing chamber of our dilution refrigerator and expose a single device (through collimators) to an ^{55}Fe/NaCl fluorescence source (Cl Kα at 2.62 keV). With this arrangement, low energy source x-rays reached our devices $\sim$ 20 times per second.

Collimated x-ray absorption events were measured using a conventional voltage-biased TES circuitry setup[6], with the W-TES sensor biased in the steepest part of its resistive transition. The total change in internal energy of a TES under such conditions is well approximated by:

$$\Delta U = \Delta U_{ext} + \Delta U_{Joule} + \Delta U_{e-ph} = 0, \qquad (1)$$

where ΔU_{ext} represents the deposited x-ray energy, ΔU_{Joule} corresponds to the Joule heating $\sim$ V^2/R of the biased TES, and ΔU_{e-ph} is an energy loss term arising from electron-phonon coupling within the TES. This latter term accounts for the thermal relaxation of the TES. It is relatively small when the TES is operated in the linear, non-saturated region of its $R(T, I)$ curve and small energy inputs are considered. In general, event energy absorbed by a voltage-biased TES will increase sensor resistance and thus decrease the instantaneous energy loss from Joule heating. When in the linear, low energy regime, the first two terms in the energy balance equation dominate the physics, and essentially cancel each other. However, when the energy flux into a TES is sufficient to drive the TES fully normal, ΔU_{e-ph} can be significant. Below, we show that by consistently including the ΔU_{e-ph} term in our model we can more accurately reproduce the observed pulse shapes and energy distributions of W-TES events in both the non-saturated and saturated regimes[7].

Fig. 2 shows the energy detected by each of the three W-TESs on a single test device exposed for $\sim$48 hours to our NaCl fluorescence source using the set-up shown in Fig. 1c. The data were obtained with a 250 μm-long Al film device similar to that shown in Fig. 1a. Event energies were determined using a non-linear optimal filter template fitting approach[7]. As shown in Fig. 2, we observed four basic classes of events: (1) x-rays absorbed directly in W-TES1 or W-TES2, (2) x-rays absorbed in the central Al film, (3) x-rays absorbed in one of the four main W/Al overlap regions of the device (one at each end of both W-TES1 and W-TES2), and most commonly (4) x-rays absorbed in the Si substrate (large W-TES3 signal). The relative count rates observed for the various event types were consistent with the source-collimator geometry and the known penetration depths[8] for 2.62 keV x-rays in Al (3.3 μm) and W (0.2 μm).

We scaled event energy measurements to the initial

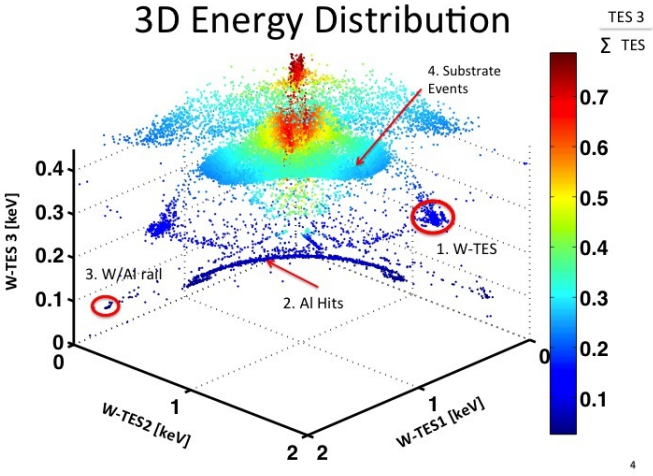

FIG. 2: (Color online) X-ray event energy collected in each of the three W-TESs of a 250 μm-long central Al film device. Four distinct x-ray interaction locations are noted: W-TES, central Al, Al/W overlap regions, and the substrate. The color bar indicates the fraction of the total detected energy appearing in the substrate channel (W-TES3). The energy collected by W-TES1 and W-TES2 for x-ray hits along the central Al film (the banana-shaped cluster of points shown) is consistent with the known device geometry.

energy stored in qps after their number became constant, *i.e.* after the initial fast phonon decay modes were complete but before qps shed sub-gap phonons[9]. In our experiments, a maximum of only 1.42 keV of the incident 2.62 keV Cl Kα x-ray energy was collected in W-TES1, even for a direct-hit in that sensor (see Fig. 2). This large energy deficit can be explained using an energy down-conversion model recently published by Kozorezov, *et.al.*[10]. Their model defines three stages of the energy down-conversion process following the absorption of an x-ray in a thin metal film. The most relevant to our experiments with W-TESs is Stage II, where athermal phonon leakage into the substrate dominates the film's energy loss to the substrate. Stage II can be subdivided into two main parts. In the first part, the mean energy of electronic excitations, ϵ, is below some threshold, E_1^*, but much higher than the Debye energy: $\Omega_D << \epsilon < E_1^*$. In this regime, energy loss to the substrate can be strongly dependent on event location in the film (*i.e.* proximity to the film-substrate boundary) and spectral peaks get broadened, but not typically shifted appreciably in energy.

The second part of Stage II is characterized by $\Omega_D > \epsilon > \Omega_1$, where Ω_1 is a low-energy threshold above which electron and hole relaxation by phonon emission is still important, but below which the dynamics is again dominated by electronic interactions. This portion of the energy cascade process turns out to be more important than expected for explaining the observed energy loss in

TESs and other film-based devices. Applying Eqs. 7, 9 and 10 of Ref.[10] to our experimental conditions yields a predicted fractional energy loss in our W films of 49% for direct-hit x-ray events. In our experiments we observe an actual energy loss of $\sim 43\%$ for these direct-hit events. One effect that can reduce this small discrepancy is the reabsorption of some high-energy escape phonons back into the W-TES from the substrate. In addition, using this energy down-conversion theory applied to our specific device geometry, x-ray events occurring in the W directly undergo more energy loss to the substrate than those occurring in the Al films (see below) resulting in a higher TES 3 signal for W.

We have developed a simple physical model that accurately describes the pulse shapes observed with our Al/W devices. We show in Fig. 3a one simulated pulse from this model superimposed on a raw pulse from a well-behaved device like the one shown in Fig. 1a. We have also used this model to reproduce previously unexplained pulse shapes[11] obtained with a device of similar design that was studied first in 1997 and then again in 2014. The same, unusual pulse shapes were observed in both data sets. The remarkable double-peak structure for that device is shown in Fig. 3b. The pulses shown come from x-ray events occurring in the central Al film.

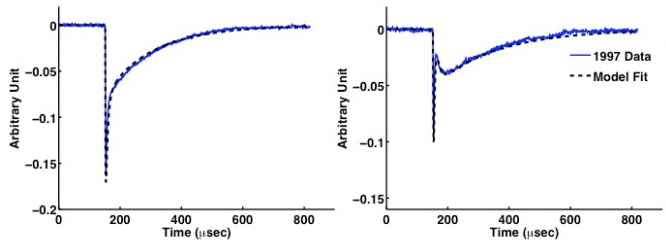

FIG. 3: (Color online) Overlay of raw data and simulated pulses for: (a) a typical Al/W test device, (b) a similar Al/W device, first tested in 1997, with odd pulse shapes that we now understand.

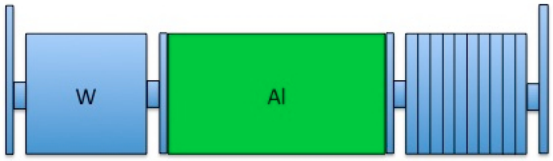

FIG. 4: (Color online) Physical model of our Al/W device that: (a) models imperfect interfaces ("waterfalls") between Al and W films as resistive links that can affect the critical current and the TES response function, and (b) treats W-TES1 and W-TES2 each as a series of ten parallel strips with thermal conductance between the strips given approximately by the Wiedemann-Franz Law.

The key elements of our physical model are shown in Fig. 4. In the model, physical weak links (i.e., multiple filamentary attachments) between the W and Al films are used to mimic the step-coverage impedance where the 40 nm-thick W film overlaps the 300 nm-thick Al film below it, as the W transitions down to the substrate where it operates as a TES (see Fig. 1b). We refer to these film transition regions as "waterfall" regions based on their appearance in SEM images[12]. In our test devices, the W/Al overlap region (Fig. 1b) is excellent along the top surface of the Al but is filamentary along the steep Al sidewalls. Our model treats the added impedance of the waterfall region as a necked-down weak W link that acts effectively as a small Joule heater providing constant power even when the W-TES itself is in its superconducting transition. This impedance alters the superconducting temperature and critical current of the TES in predictable ways. Additionally, instead of treating the W-TES as a lumped element, in our model each TES square is divided into ten equal-width strips parallel to the W/Al overlap region. The heat capacity of each strip is assumed to be the same as all others. The Wiedemann-Franz Law is then used in a one-dimensional (1D) simulation of qp thermalization in the voltage-biased TES as energy flows through it laterally[7].

Our waterfall model works well. For example, it yields the first decay-time in the raw data pulse shown in Fig. 3a. It also correctly predicts the second distinct decay-time that corresponds to the time (τ_{etf}) needed for the TES to cool back to its equilibrium state. Lastly, the model explains the double-peaked pulses observed with our older devices from 1997 - the odd pulse shapes we now know resulted from poor film connectivity between each W-TES and its corresponding Al bias line at the end away from the main Al absorber (see Fig. 4). We have shown that the poor connectivity between the TES and the Al x-ray absorber film is due to sputtering geometry[13]. The subset of devices that exhibited the odd pulse shape shown in Fig. 3b were found to have poor connectivity at the wiring side of the TES, caused by mask misalignment and etch problems during fabrication. A detailed description of this model and its use in pulse shape simulations is discussed in Ref.[7].

After selecting Al direct-hit events (dark blue in Fig. 2) using the method described in Ref.[12], we modeled qp transport in the Al film using a 1D diffusion equation with a linear loss term:

$$\frac{\partial n}{\partial t} = D_{\rm Al}\frac{\partial^2 n}{\partial x^2} - \frac{n}{\tau_{\rm Al}} + s, \qquad (2)$$

where $n = n(x,t)$ is the linear number density of qps, $D_{\rm Al}$ is the diffusivity of qps, and $\tau_{\rm Al}$ is the qp trapping time. The source term $s = q\,\delta(x-x_0)\delta(t-t_0)$ represents the rate of qp density creation. The rates for qp absorption into W-TES1 and W-TES2, symbolized by I_1 and I_2 respectively, were modeled by the linear relations:

$$I_1 = n_1\,v_1, \quad I_2 = n_2\,v_2, \qquad (3)$$

where the coefficient $v_1(v_2)$ has units of length/time, and n_1 (n_2) is the qp number density at the W/Al boundary

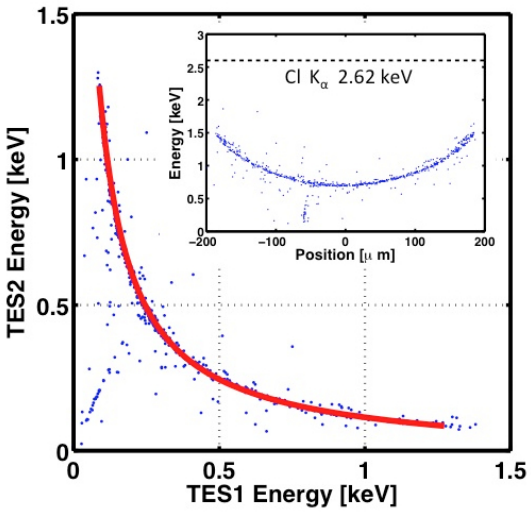

FIG. 5: (Color online) Overlay of raw energy collection distribution and Maximum Likelihood fit. The banana-shaped cluster of points corresponds to direct-hit x-rays in the main Al film. (Inset): Collected x-ray energy vs. event location along the Al film. The cluster of points near -55μm is consistent with x-rays absorbed in the ground line of the main Al film. These data correspond to events with pulse shapes like that shown in Fig. 3a.

closest to W-TES1 (W-TES2). This 1D approach is sufficient because the qps are reflected at the edges of the Al, and the mean free path is smaller than the width of the film, making diffusion along the two axes independent.

Equation 2 can be solved analytically to find the fraction $F_1(F_2)$ of qp generated by an event that is absorbed in W-TES1(W-TES2):

$$F_1 = \frac{\Lambda_d \left(\lambda_2 \cosh\left(\frac{1+2\xi}{2\Lambda_d}\right) + \Lambda_d \sinh\left(\frac{1+2\xi}{2\Lambda_d}\right)\right)}{\Lambda_d(\lambda_1+\lambda_2)\cosh\left(\frac{1}{\Lambda_d}\right) + (\Lambda_d^2+\lambda_1\lambda_2)\sinh\left(\frac{1}{\Lambda_d}\right)} \quad (4)$$

$$F_2 = \frac{\Lambda_d \left(\lambda_1 \cosh\left(\frac{1-2\xi}{2\Lambda_d}\right) + \Lambda_d \sinh\left(\frac{1-2\xi}{2\Lambda_d}\right)\right)}{\Lambda_d(\lambda_1+\lambda_2)\cosh\left(\frac{1}{\Lambda_d}\right) + (\Lambda_d^2+\lambda_1\lambda_2)\sinh\left(\frac{1}{\Lambda_d}\right)} \quad (5)$$

The dimensionless variable $\Lambda_d \equiv L_d/L$ depends on the characteristic diffusion length $L_d = \sqrt{D_{\rm Al}\tau_{\rm Al}}$ of the Al film, and the term $\xi \equiv x_0/L$ depends on the qp source location, x_0, measured from the center of the Al film. L is the length of the Al film. The dimensionless parameters λ_1 and λ_2 are defined by the relation, $\lambda_i \equiv L_i/L$, where $L_i = D_{\rm Al}/v_i$ $(i = 1, 2)$ is a characteristic qp absorption parameter with units of length that varies inversely with the efficiency for coupling qp into each W-TES. In general the W-TESs would have slightly different qp absorption capabilities, hence $\lambda_1 \neq \lambda_2$. However, if one assumes the same absorption capability for the two TESs, Eq. 4 and Eq. 5 can be further simplified to the form shown in Eq. 1 of Ref.[1].

Fig. 5 shows a Maximum Likelihood fit of this diffusion model to x-ray data for a 350 μm-long Al film. The fit yields estimates for three important parameters: the characteristic qp diffusion length, L_d, the qp absorption into W-TESs, $L_1(L_2)$, and an energy scaling factor, $\mathcal{E}_{\rm sf}$. The scaling factor corresponds to the deposited energy before position dependent qp trapping and sub-gap phonon losses have occurred as energy is absorbed into the two W-TESs. Applying Eq. 2 to our data yields $L_{\rm d} \sim 130\mu$m for three Al film lengths studied: 250 μm, 350 μm, and 500 μm. For small values of L_i, the band of Al direct-hit events shown in Fig. 5 would extend towards the energy axes. In our data, $L_1 \approx L_2 \sim$100 μm, and we observe gaps between the end points of the Al direct-hit band and the energy axes. Summing the two W-TES energies and reconstructing position yields the inset of Fig. 5. Note that individual values of $D_{\rm Al}$ and $\tau_{\rm Al}$ cannot be determined using Eq. 2 alone. In the next paper, we will determine $D_{\rm Al}$ and $\tau_{\rm Al}$ separately using TES time-delay data and different thickness Al films.

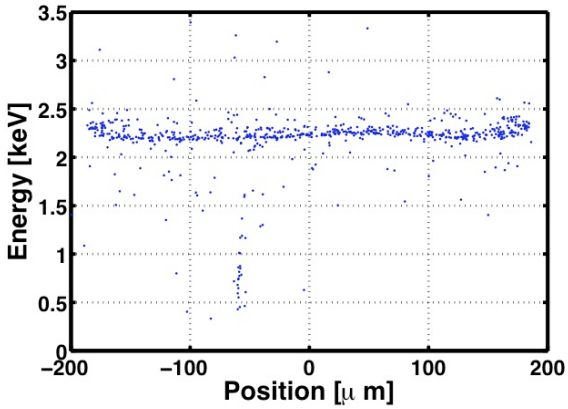

FIG. 6: Reconstructed Cl K$_\alpha$ x-ray energy as a function of event position along Al film. This corresponds to the deposited energy before position dependent qp trapping and sub-gap phonon losses have occurred.

Fig. 6 shows the reconstructed energy vs. position data of Fig. 5 using the parameters from our diffusion model fit. The scaling factor obtained from the model yields a total event energy of 2.3 keV rather than the expected 2.62 keV. This $\sim$ 10% discrepancy is consistent with known energy down-conversion mechanisms[10]. The 5% variation in reconstructed energies shown in Fig. 6 can be corrected using a model that includes the latter stages ($\epsilon < 3\Delta$) of the energy down-conversion cascade and simulates qp trapping in terms of a percolation threshold (below which qps are trapped by local variations in the gap)[14]. Electronic and environmental noise sources in lab currently limit our energy resolution for $\sim$ 6 keV x-rays to $\sim$ 100 eV FWHM for events in the Al film and 50 eV for W-TES "direct-hit" events.[7].

The results presented here for x-rays interacting with Al films coupled to W-TESs are useful for optimizing CDMS detector performance, which improves for large

Al film qp diffusion lengths and well-coupled Al and W films at all W-TES interfaces. The response function of a TES relates closely to its critical current. For the CDMS array of ~ 2.5 μm wide TESs in parallel, connections to the ends of the TESs are typically ~ 33 μm wide. For our test devices, the Al and W films have equal width. Thus, our test devices are $\sim$ 13 times more sensitive to critical current issues due to filamentary "waterfalls" than comparably fabricated CDMS QETs. These studies also allow us to monitor the fabrication integrity and catch defect levels that do impact CDMS detector performance.

A simple model fit to our data matches the observed pulse shapes well, and correctly determines the energy of direct-hit events in W-TESs. Our results are consistent with phonon and qp energy down-conversion physics. In the simple diffusion model used here, losses to sub-gap phonons and qp trapping were combined into a single, generic term. A more detailed study that includes percolation threshold effects from spatial variations in the superconducting gap of our Al films will be reported soon.We are also using SEM and FIB imaging to modify fabrication recipes and improve connectivity at the Al/W interfaces[13].

ACKNOWLEDGMENTS

We thank the Stanford Physics Machine Shop staff for making source and sample holders, and collimators. We thank K. D. Irwin and S. Chaudhuri for useful discussions on TES physics. We also thank M. Pyle and K. Schneck for CDMS related conversations. The authors would also like to thank A. Kozorezov and S. Bandler for useful qp and phonon physics discussions. We acknowledge support from the Department of Energy, DOE grant DE-FG02-13ER41918, and the National Science Foundation, NSF grant PHY-1102842.

[1] M. Loidl, S. Cooper, O. Meier, F. Pröbst, G. Sáfrán, W. Seidel, M. Sisti, L. Stodolsky, S. Uchaikin, *Nucl. Instr. and Meth. A,* **465**, 440-446, (2001).

[2] J. Martin, S. Lemkea, R. Grossa, R.P. Huebenera, P. Videlerb, N. Randob, T. Peacockb, P. Verhoeveb, F.A. Jansenb, *Nucl. Instrum. Methods A* **370**, 88-90, (1996).

[3] C. Bailey, J. Adams, S. Bandler, J. Chervenak, M. Eckart, A. Ewin, F. Finkbeiner, R. Kelley, C. Kilbourne, F. Porter, J. Sadleir, S. Smith, M. Sultana, *J. Low Temp.* **167**, 3-4, (2012).

[4] Z. Ahmed, D. S. Akerib, S. Arrenberg, C. N. Bailey, D. Balakishiyeva, L. Baudis, D. A. Bauer, P. L. Brink, T. Bruch, R. Bunker, *et al.*, *Phys. Rev. Lett.* **106**, 131302, (2011).

[5] N. E. Booth, *Appl. Phys. Lett* **50**, 293, (1987).

[6] K. D. Irwin, S. W. Nam, B. Cabrera, B. Chugg and B. A. Young, *Rev. Sci. Instrum.* **66**, 5322, (1995).

[7] B. Shank, J. J. Yen, B. Cabrera, J. M. Kreikebaum, R. Moffatt, P. Redl, B. A. Young, P. L. Brink, M. Cherry, A. Tomada, submitted to *AIP Advances.*

[8] S. M. Seltzer, *Radiation Research.* 136 (1993).

[9] Guruswamy, D J Goldie and S Withington, *Supercond. Sci. Technol.* **27**, 055012 (2014).

[10] A. G. Kozorezov, C. J. Lambert, S. R. Bandler, M. A. Balvin, S. E. Busch, P. N. Nagler, J. P. Porst, S. J. Smith, T. R. Stevenson, and J. E. Sadleir, *Phys. Rev. B* **87**, 104504, (2013).

[11] M. Pyle, P. L. Brink, B. Cabrera, J. P. Castle, P. Colling, C. L. Chang, J. Cooley, T. Lipus, R. W. Ogburn, B. A. Young, *Nucl. Instrum. Methods A* **559**, 405, (2006).

[12] J. J. Yen, B. A. Young, B. Cabrera, P. L. Brink, M. Cherry, R. Moffatt, M. Pyle, P. Redl, A. Tomada and E. C. Tortorici *Journal of Low Temp. Phys.* **176**, 168-175, (2014).

[13] J. M. Kreikebaum, B. A. Young, B. Cabrera, P. L. Brink, M. Cherry, A. Tomada, J. J. Yen, submitted to *Journal of Vacuum Society and Technology B.*

[14] B. Cabrera, in preparation.